LF



MET O 11 TECHNICAL NOTE NO. 160

# Solutions to a model of a front forced by deformation

M.J.P. Cullen



Meteorological Office,
Met O 11
London Road,
Bracknell,
Berkshire, RG12 2SZ

July 1982

Summary

The deformation model of a front studied by Hoskins and Bretherton (1972) is studied further. It is shown that a unique solution of the Lagrangian conservation laws governing the motion can still be constructed after the front has formed. This solution shows that separate upper and lower fronts propagate into the fluid, and are separated by a region where only smooth variations occur. Finite difference solutions are also given which converge to a front with the correct mean slope and maximum long front velocity but without the correct variation in slope through the depth of the fluid.

## 1. INTRODUCTION

A great deal of theoretical work has been carried out on the problem of atmospheric frontogenesis. This problem contains interesting mathematical features, in particular the tendency to collapse to a discontinuity in certain variables, as well as being physically important. The mathematical work on this problem has been recently reviewed by Hoskins (1982). It is possible to construct approximate systems of equations whose solutions indicate a tendency to form discontinuities in a finite time. These discontinuities appear first on boundaries, or at discontinuities in potential vorticity, such as the tropopause. In the case of upper tropospheric fronts, folding of the tropopause inhibits formation of the discontinuity. The detailed mathematics used to derive these results is set out in Hoskins and Bretherton (1972), henceforward referred to as HB.

It is a common situation in computational fluid dynamics for the solution to an inviscid set of model equations to become discontinuous, and for the physical dissipation scale to be several orders of magnitude smaller than the grid-length that can be used. In some problems it is possible to prove that a discontinuous solution to the inviscid problem is the limit as the viscosity tends to zero of the viscous problem. Such results exist for many one dimensional systems of conservation laws, eg Chorin and Marsden, (1979). After the solution becomes discontinuous the differential equations are no longer meaningful, and must be replaced by a statement of the physical conservation principles from which they were derived. It is important to select the correct conservation laws, or the result will disagree with experiment. In most cases the conservation laws are not sufficient to determine the solution uniquely, and extra conditions are required to exclude unphysical solutions. For instance, a discontinuous solution to the shallow water equations can be obtained uniquely by requiring conservation of mass and momentum, and a decrease of the total energy. When solving inviscid

equations numerically, artificial viscosity has to be used to smear any discontinuities over a grid length. In order that the correct physical solution is obtained, subject to the smearing, the correct conservation laws must be exactly satisfied, and the required extra conditions enforced. An example of how this can be done is given by Majda and Osher (1979) for the Lax Wendroff scheme.

This paper attempts to derive such a discontinuous solution for one of the inviscid models of frontogenesis discussed by HB. We consider the simplest case, that of a front forced by a deformation field in a fluid of zero potential vorticity confined between rigid upper and lower boundaries. Such a front forms the boundary between air masses of different potential temperatures and thus no fluid can cross it. It is therefore a contact discontinuity. The presence of the front should thus not invalidate Lagrangian conservation laws, which follow fluid particles. However it will invalidate the Eulerian form of the inviscid differential equation. In HB it was shown that the inviscid semi-geostrophic equations could be completely written in the form of Lagrangian conservation laws. In this paper we show how a solution of these laws can be constructed in the presence of a discontinuity.

Such a solution turns out to have non-trivial structure. Fronts are initially formed at both the upper and lower boundaries. However a single front through the full depth of the fluid can never be formed. This is because of the conservation of mass of parcels of air having intermediate values of potential temperature. These parcels can only be reduced in cross-section by the basic deformation field; and they can not thus be eliminated in a finite time. The solution thus consists of a split front, with a region in the middle troposphere where only smooth variations occur.

A standard finite difference solution is then carried out using the primitive equations rather than the semi-geostrophic equations used in HB. The discontinuous solution derived to the semi-geostrophic equations should be a limit of the solution of the viscous primitive equations as the rotation rate increases and the viscosity tends to zero. Taking either of these limits may result in the solution becoming singular and it is therefore important that the limits are taken in the correct order. As discussed in HB, the approximation of no mixing breaks down, because of the onset of turbulence, before the semi-geostrophic approximation breaks down. Thus it is to be expected that the solution obtained by making the semi-geostrophic approximation and then letting the viscosity tend to zero will be physically correct.

The computations show that a finite difference solution to the primitive equations with artificial viscosity converges to a solution with the correct total frontal thickness and maximum long front velocity. However, the vertical structure of the front is largely missing. The convergence rate is very slow and 5 km resolution with 40 or 60 vertical levels is required to make the front sharp even at the boundaries. It is not certain whether the failure to obtain any vertical structure is because even higher resolution is required or that the finite difference scheme does not converge to the solution of the Lagrangian conservation laws. It is also possible that the finite difference scheme is converging to an inviscid solution of the primitive equations which is different from an inviscid solution of the semi-geostrophic equations, because of the different order in which the limits are taken.

## 2. SOLUTION OF THE SEMI GEOSTROPHIC EQUATIONS

We solve an essentially two dimensional set of equations, using the Boussinesq approximation, as in HB:

$$\frac{\partial u}{\partial t} + u\frac{\partial u}{\partial x} + w\frac{\partial u}{\partial z} + \frac{\partial \phi}{\partial x} - fv = 0$$

$$\frac{\partial v}{\partial t} + u\frac{\partial v}{\partial x} + \alpha v + w\frac{\partial v}{\partial z} + f(\alpha x + u) = 0$$

$$\frac{\partial u}{\partial x} + \alpha + \frac{\partial w}{\partial z} = 0 \qquad (2.1)$$

$$\frac{\partial \theta}{\partial t} + u\frac{\partial \theta}{\partial x} + w\frac{\partial \theta}{\partial z} = 0$$

$$\frac{\partial \phi}{\partial z} = g\theta/\theta_0$$

$$w = 0 \quad \text{at} \quad z = 0, H$$

These are obtained from the full equations by assuming

$$u = -\alpha x + u'(x,z,t)$$

$$v = \alpha y + v'(x,z,t) \qquad (2.2)$$

$$\phi = f\alpha xy - \alpha^2 y^2/2 + \phi'(x,z,t)$$

and solving in the plane y = 0.

The initial conditions in the plane $y = 0$ are:

$$u = -\alpha x$$

$$v = f(X(x,z) - x)$$

$$\theta(x,z) = \theta_0 + \theta_1 \tan^{-1}\left(\frac{\pi X(x,z)}{L}\right) \qquad (2.3)$$

where

$$\frac{x - X(x,z)}{z - \frac{1}{2}H} = -\frac{\pi\theta_0\theta_1}{gL}\frac{1}{\left(1 + \left(\frac{X(x,z)}{L}\right)^2\right)} \qquad (2.4)$$

The boundary conditions at $x = \pm L$ are

$$\begin{aligned} u &= \mp \alpha L \\ v &= 0 \\ \theta &= \theta_0 \pm \theta_1 \tanh^{-1}(S) \end{aligned} \tag{2.5}$$

The particular choice of the initial condition (2.3) makes the potential vorticity zero as will be explained later.

The equations (2.1) are solved in the Lagrangian form used by HB. The equations for $v$ and $\theta$ can be written in the form:

$$\begin{aligned} \frac{D(v+fx)}{Dt} + \alpha(v+fx) &= 0 \\ \frac{D\theta}{Dt} &= 0 \end{aligned} \tag{2.6}$$

where $$\frac{D}{Dt} \equiv \frac{\partial}{\partial t} + u\frac{\partial}{\partial x} + w\frac{\partial}{\partial z}.$$

Defining the absolute momentum M as $(v + fx)$, this gives

$$\begin{aligned} \frac{DM}{Dt} + \alpha M &= 0 \\ \frac{D\theta}{Dt} &= 0 \end{aligned} \tag{2.7}$$

In HB, the semi-geostrophic approximation is now made, which reduces the first equation in (2.1) to

$$\frac{\partial \psi}{\partial x} = fv \tag{2.8}$$

Under this assumption, they show that the motion is completely specified by (2.7) and

$$\frac{Dq}{Dt} = 0 \tag{2.9}$$

where $$q = \frac{\partial(M,\theta)}{\partial(x,z)}$$

$q$ is the potential vorticity.

The initial data (2.3) satisfies the condition that surfaces of constant $M$ and constant $\theta$ coincide, with slope $$-\frac{S\theta_0\theta_1}{gL(1+(x/L)^2)}$$ with $X$ as defined by (2.4). This means that $q=0$ everywhere initially. In HB a solution to this problem is then constructed from the information that surfaces of constant $M$ and $\theta$ must coincide for all time. The slope of these surfaces is given by

$$-\frac{f\theta_0}{g}\frac{\partial M}{\partial \theta} \qquad (2.10)$$

In addition, because of the incompressibility condition under the Boussinesq approximation, and the rigid upper and lower boundaries, the area $A(\Delta\theta)$ of fluid with values of $\theta$ in a prescribed range $\Delta\theta$ obeys the equation

$$\frac{\partial A(\Delta\theta)}{\partial t} = -\alpha A \qquad (2.11)$$

Thus as the sloping surfaces bounding this fluid element change slope; they must do so in such a way that its area satisfies (2.11).

We now generalise this procedure to cover the case where a discontinuity has formed. Though mixing will take place on small scales where there is a near discontinuity, it is reasonable to seek a discontinuous solution to describe the large scale pattern. Since $\theta$ is conserved following a particle the discontinuity must be a contact discontinuity, which no fluid crosses. Thus we approximate a general $\theta$ distribution by a piecewise constant distribution as shown in Fig. 1, in the spirit of the method used by Glimm (1965) to prove the

existence of solutions to hyperbolic conservation laws. Since $M$ and $\theta$ surfaces coincide, we assume that the distribution of $M$ is also piecewise constant. Segments in which $M$ and $\theta$ are constant are separated by straight lines in the $(x, z)$ plane with slope

$$-\frac{f\theta_0}{\delta}\frac{[M]}{[\theta]} \qquad (2.12)$$

where $[M]$, $[\theta]$ are the differences in $M$ and $\theta$ between the segments. The area of each segment changes with time according to (2.11).

Up till the formation of a discontinuity, the lines separating the segments change slope and converge at either the upper or lower boundary (Fig. 2); but all dividing lines intersect both boundaries. Once they meet, in order that the conservation laws (2.7), (2.9) and (2.11) remain satisfied, some of the segements are forced away from the boundaries. The evolution is depicted diagramatically in Figs 3 and 4. The slopes of surfaces separating each pair of segments still satisfy (2.12), but because the frontal surface separates different segments as it leaves the boundary, it is not straight. The conservation of area, (2.11), means that a single front cannot be formed through the depth of the fluid, as otherwise some segments would have to vanish. Inspection of Figs. 2 to 4 shows that there is no difficulty in constructing a pattern of segments at each time, so that each is bounded by lines with the correct slope and has the correct area. However, to prove rigorously that this is possible for all time would be very difficult.

This procedure allows a solution to be computed diagnostically at any given time as follows:

(i) Given initial segments with potential temperatures $\{\theta_n\}$, absolute momenta $\{M_n\}$, and areas $\{A_n\}$; the values of these quantities at time $t$ are respectively $\{\theta_n\}$, $\{M_n e^{-\lambda t}\}$, $\{A_n e^{-\lambda t}\}$.

(ii) Calculate the slope of the boundary between adjacent segments using (2.12).

(iii) Seek a pattern as shown in Figs. 2 to 4, allowing all the segments to be fitted in. Once the discontinuity has formed, extra logic is required to determine which segments adjoin and what the resulting frontal slope is. Calculating this requires some iteration. Since the calculation is symmetrical, the pattern can be built in from both ends $x = \pm L$. The detailed logic is a very ad-hoc procedure which requires guessing which segments adjoin, and then calculating exact positions of the boundaries to give the correct areas and slopes. If no solution is found for a given arrangement of segments, other arrangements are tested until all the conditions can be satisfied.

The solution obtained this way is a discontinuous solution of the Lagrangian conservation laws (2.7), (2.9) and (2.11). Since the discontinuity is a contact discontinuity, there is no reason to suppose that these laws will break down, since no particle actually crosses the discontinuity. It is therefore reasonable to hope that this is the correct physical limiting solution as the viscosity tends to zero. Whether this is actually so can only be determined by experiment.

## 3. FINITE DIFFERENCE SOLUTION OF THE PRIMITIVE EQUATIONS

We now seek to establish whether a standard finite difference solution of equations (2.1) to (2.4) converges to the solution of the semi-geostrophic equations discussed above as the mesh is refined. In order to handle the discontinuity, artificial viscosity terms of the form $K\frac{\partial^2 u}{\partial x^2}$ are added to the equations for $u$, $v$ and $\theta$ in (2.1). The equations are then approximated by a standard semi-implicit finite difference scheme; using a staggered grid as shown in Fig. 5. In the usual notation:

$$\delta_x A = \left( A\left(x + \tfrac{1}{2}\Delta x\right) - A\left(x - \tfrac{1}{2}\Delta x\right)\right)/\Delta x$$

$$\overline{A}^{x} = \tfrac{1}{2}\left( A\left(x + \tfrac{1}{2}\Delta x\right) + A\left(x - \tfrac{1}{2}\Delta x\right)\right)$$

$$\overline{A}^{2x} = \tfrac{1}{2}\left( A(x + \Delta x) + A(x - \Delta x)\right)$$

the scheme is

$$\delta_t \bar{u}^t + \overline{\bar{u}^x(\delta_x u)}^x + \overline{\bar{w}^x(\delta_z u)}^z + \delta_x(\phi - \phi_*) + \overline{\delta_x \phi_*}^{2t} - f\bar{v}^x = K_u \delta_x \delta_x u \tag{3.1}$$

$$\delta_t \bar{v}^t + \overline{u \delta_x v}^x + dv + \overline{w \delta_z v}^z + f dx + f\bar{u}^x = K_v \delta_x \delta_x v \tag{3.2}$$

$$\delta_x u + d + \delta_z w = 0 \tag{3.3}$$

$$\delta_t \bar{\theta}^t + \overline{u(\delta_x \theta)}^x + \overline{w \delta_z \theta}^z = K_\theta \delta_x \delta_x \theta \tag{3.4}$$

$$\delta_z \phi = g \bar{\theta}^z / \theta_0 \tag{3.5}$$

$$\phi = \phi_* \quad \text{at} \quad z = 0 \tag{3.6}$$

$$w = 0 \quad \text{at} \quad z = 0, H \tag{3.7}$$

$$\left.\begin{aligned} u &= \pm d(L - \tfrac{1}{2}\Delta x) \\ v &= 0 \\ \theta &= \theta_0 \pm \tan^{-1}(S) \end{aligned}\right\} \quad \text{at} \quad x = \pm L \tag{3.8}$$

The time averaged term $\overline{\delta_x \phi_*}^{2t}$ in (3.1) makes the scheme implicit. Equation (3.3), together with the boundary condition $w=0$ at $z=0$, is first used to calculate $w$. Equation (3.5), with $\phi$ set equal to zero at $z=0$, is used to calculate $\phi$. Equation (3.1) with the term in $\overline{\phi_*}^{2t}$ omitted, and equations (3.2) and (3.4) are then solved for $u^*(t+\Delta t)$, $v(t+\Delta t)$, $\theta(t+\Delta t)$. The resulting values of $u^*$ will not satisfy the integral of (3.3), which states that

$$n d + \sum_{i=1}^{\wedge} \delta_x u = w(0) - w(H) = 0 \tag{3.9}$$

where $\wedge$ is the number of grid points between $z=0$ and $H$ and the summation is in the vertical. We therefore seek values of $\phi_*(x)$ such that $(u^*(t+\Delta t) - 2\Delta t \delta_x \phi_*)$ satisfies (3.9).

This requires

$$n\alpha + \sum_{i=1}^{n} \delta_x u^n(t+\Delta t) - 2\Delta t n \delta_x \delta_x \phi_n = 0 \qquad (3.10)$$

In order to solve (3.10), we require boundary conditions on $\phi_n$. Since $u$ is specified at $x = \pm(L - \frac{1}{2}\Delta x)$, these are

$$\delta_x \phi_n = 0 \quad \text{at} \quad x = \pm(L - \tfrac{1}{2}\Delta x) \qquad (3.11)$$

Conditions (3.11) are consistent with (3.10) provided that

$$u^n(L - \tfrac{1}{2}\Delta x) - u^n(-L + \tfrac{1}{2}\Delta x) = 2\alpha(L - \tfrac{1}{2}\Delta x)$$

which is ensured provided that (3.1) is not used to increment $u$ at these points. In this case, (3.10) can be solved by a straightforward tridiagonal inversion.

## 4. RESULTS

Solutions are shown for equations (2.1) in a domain of length 2L = 1000 km with height H = 10 km. The initial data is given by (2.3) and (2.4) with $\theta_0 = 300^\circ K$ and $\theta_1 = 1^\circ K$. The Coriolis parameter $f$ is $10^{-4}$. The solutions to the Lagrangian equations can be derived almost exactly; the only possible error is due to the iteration on the slope of the frontal surface as discussed in section 2. However, in order to use standard plotting routines, the solutions have to be transferred to a grid. The interpolation procedure in the plotting program is not local, and therefore the results appear to contain wiggles in some places. These should be ignored, since the solution qualitatively looks like Figs. 1 to 4 with straight lines separating the segments.

Finite difference solutions are shown using grids of 100 x 10, 200 x 20, 100 x 60 and 200 x 40 points. These give horizontal resolutions of 10 km and 5 km. Results are shown after 13.9 hours. Figs. 6 to 12 show the potential temperature field and Figs. 13 to 19 the long-front velocity field for the following calculations:

(i) Exact solution extracted to a grid.

(ii) Finite difference solution on 100 x 10 grid, with an artificial viscosity coefficient, $K$ , of $10^5$ $m^2 sec^{-1}$ for all fields.

(iii) Solution on 100 x 10 grid with $K = 5 \times 10^4$.

(iv) Solution on 200 x 20 grid with $K = 2.5 \times 10^4$

(v) Solution on 200 x 20 grid with $K = 1.25 \times 10^4$

(vi) Solution on 100 x 60 grid with $K = 1.25 \times 10^4$

(vii) Solution on 200 x 40 grid with $K = 1.25 \times 10^4$

The solutions for the potential temperature field show a steady convergence towards the reference solution as the resolution is increased to 200 x 20 points and the viscosity reduced. The front, which is spread almost uniformly through the depth of the fluid in Fig. 7, is concentrated at the boundaries in Fig. 10. However, as the resolution is increased further, (Figs. 11, 12), the detail of the change in slope of the frontal surface to a lower value in the middle of the fluid is still not captured, and has not improved from Fig. 10. The overall width of the frontal region is correct. The results for the long front velocity show a steady increase as the resolution is increased, the maximum value at the highest resolution is within 10% of the correct value.

The differences between the finite difference solution and the exact Lagrangian solution are significant, but are not likely to have an impact on the feedback to larger scales, since the frontal width and maximum velocity are correct. The failure to obtain the correct change in slope through the depth of the fluid could be important when a more complete problem, for instance including moisture, was solved. The most likely reason for the failure is that the temperature contrast always has to be spread over a few grid points; and that the jump condition (2.12) which determines the slope is never calculated using the full values of the jumps $[M]$ , $[\theta]$ across the front, but only using differences between adjacent grid-points. If it turned out that the details of the slope were dynamically important, then some action would be required to solve the problem.

## 5. DISCUSSION

This paper demonstrates that a discontinuous solution of the two dimensional deformation model of a front can be uniquely constructed and is determined by large-scale information. This is thus an example of a problem where the generation of small scales does not destroy the predictability of the large scales. It is not possible, of course, to prove that this is the physically correct solution. That can only be done by carrying out a laboratory experiment. The finite difference solution converges to a solution with the correct mean slope, but does not appear to be able to predict the variation in slope with height. In the atmosphere, this failure may not matter, because the real structure of a front is much more complex than this simple model; and a great deal of further work is required to see if that real structure is correctly represented in numerical models. This paper is only a first step in this direction.

References


Chorin, A J and Marsden, J E 1979 A mathematical introduction to fluid mechanics. Springer-Verlag, 205 pp.

Glimm, J 1965 Solutions in the large for non-linear hyperbolic systems of equations. Communications on Pure and Applied Mathematics, 18, p. 697.

Hoskins, B J 1982 The mathematical theory of frontogenesis. To appear.

Hoskins, B J, and Bretherton, F P 1972 Atmospheric frontogenesis models: mathematical formulation and solution. J Atmos. Sci., 29, 11-37.

Majda, A and Osher, S 1979 Numerical viscosity and the entropy condition. Comm. Pure. Appl. Math. 32, 797-838.


List of figures

Fig. 1 Typical initial distribution of segments.

Fig. 2 Distribution of segments at the formation of a discontinuity.

Fig. 3 Evolution of the discontinuity.

Fig. 4 As Fig. 3, for a later time.

Fig. 5 Staggered grid used for finite difference calculations.

Fig. 6 Exact solution at 13.9 hr, potential temperature.

Fig. 7 Potential temperature at 13.9 hr, 100 x 10 grid, $K = 10^5\ m^2 s^{-1}$.

Fig. 8 As Fig. 7, $K = 5 \times 10^4\ m^2 s^{-1}$.

Fig. 9 As Fig. 8, 200 x 20 grid, $K = 2.5 \times 10^4\ m^2 s^{-1}$.

Fig. 10 As Fig. 9, $K = 1.25 \times 10^4\ m^2 s^{-1}$.

Fig. 11 As Fig. 10, 100 x 60 grid.

Fig. 12 As Fig. 11, 200 x 40 grid.

Fig. 13 Exact solution at 13.9 hr, long-front wind.

Fig. 14 As Fig. 7, long-front wind.

Fig. 15 As Fig. 8, long-front wind.

Fig. 16 As Fig. 9, long-front wind.

Fig. 17 As Fig. 10, long-front wind.

Fig. 18 As Fig. 11, long-front wind.

Fig. 19 As Fig. 12, long-front wind.

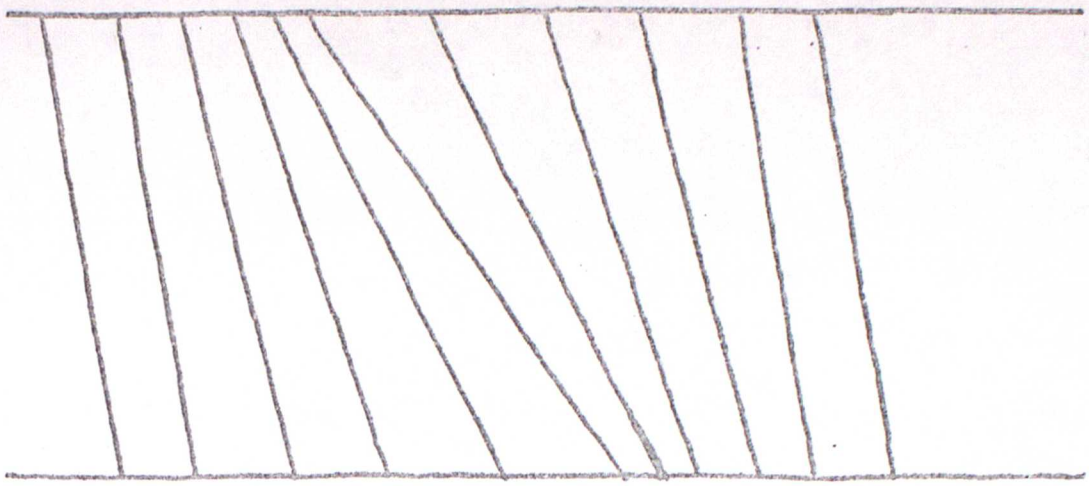

Figure 1.

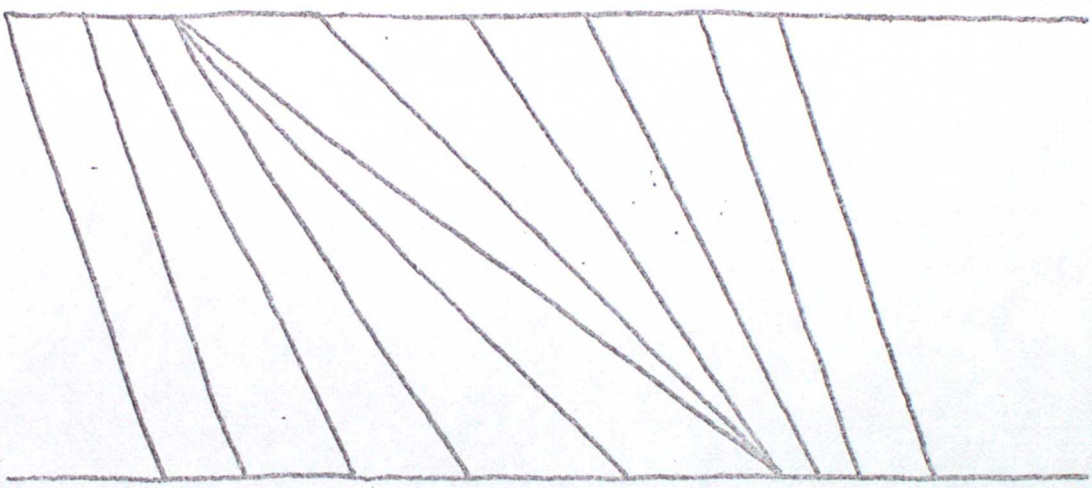

Figure 2.

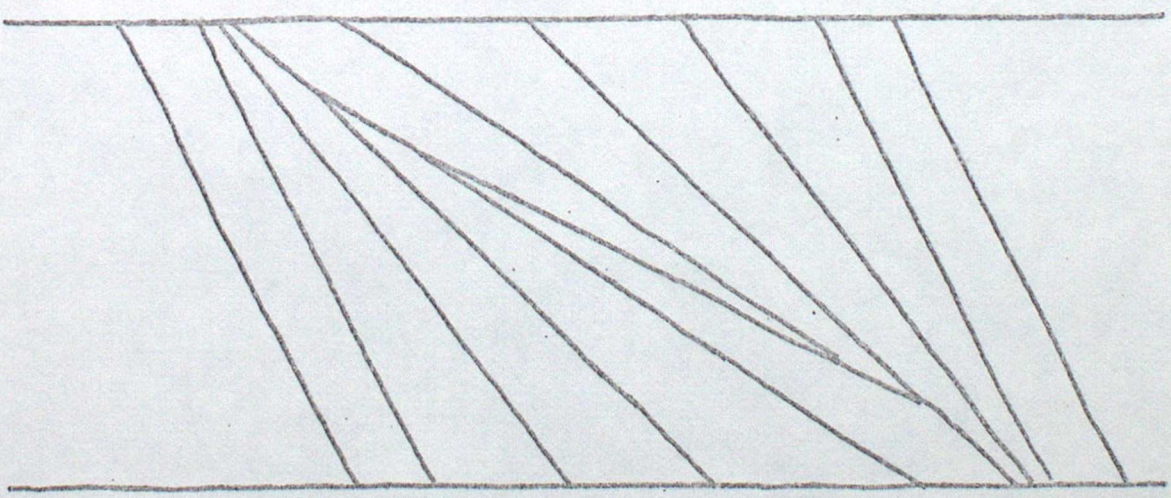

Figure 3.

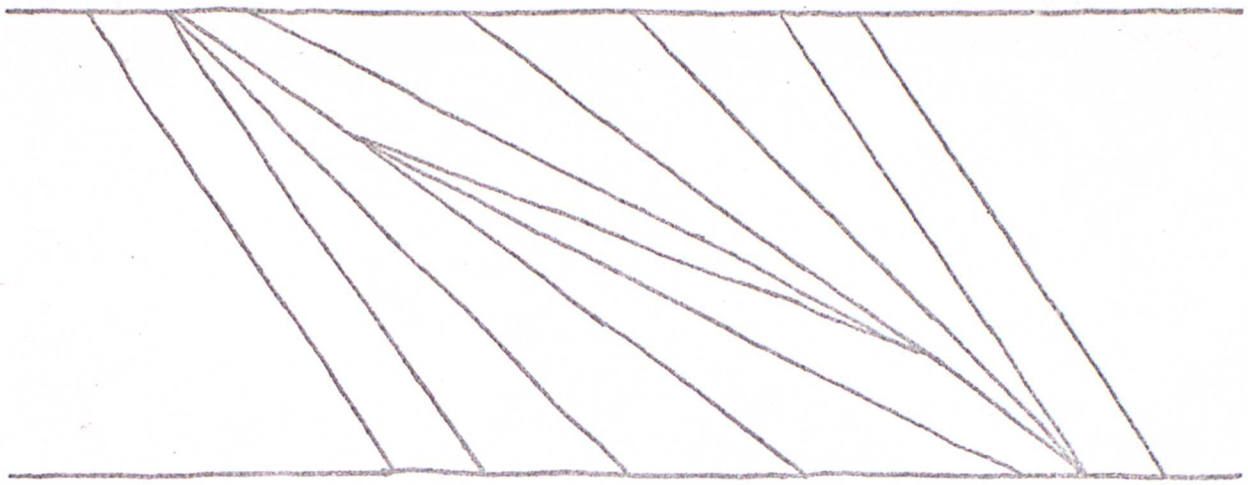

Figure 4.

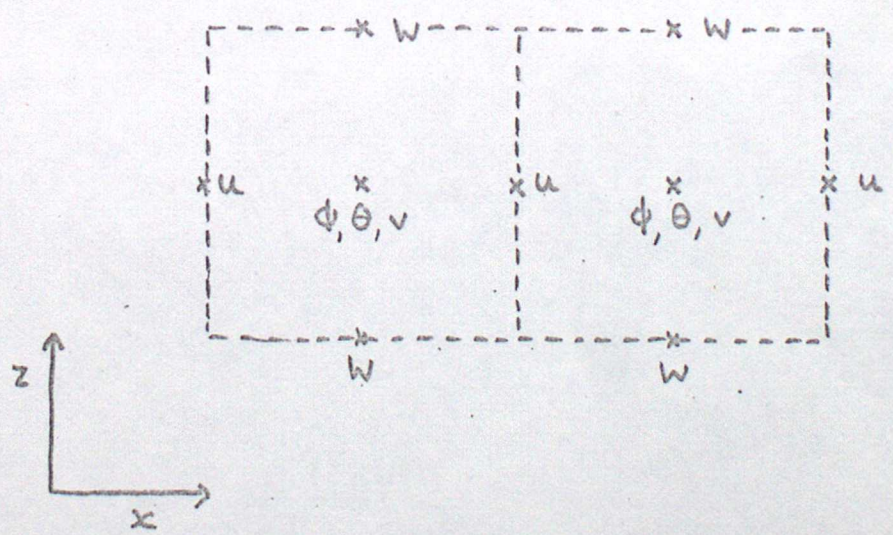


Figure 5.

Figure 6.

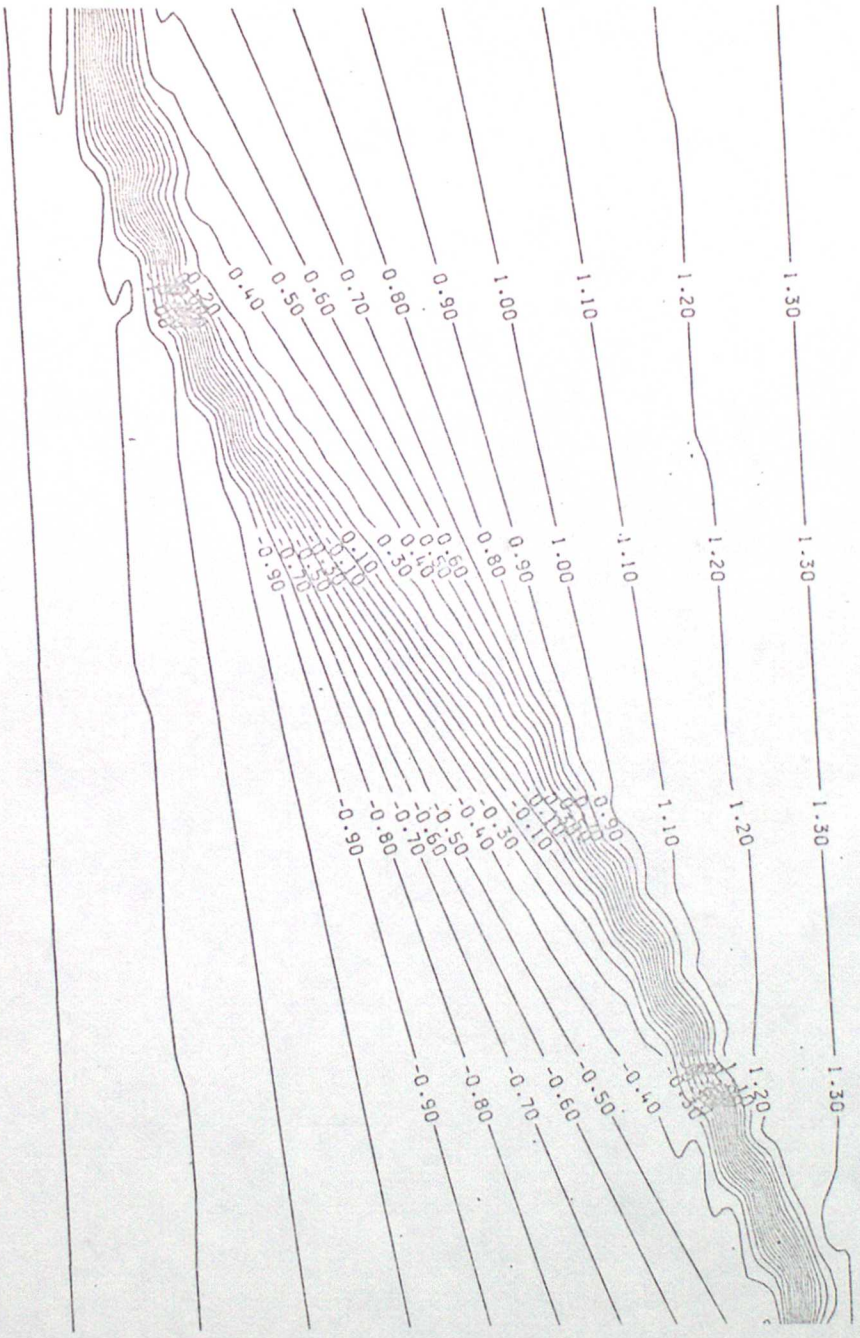
0.40
0.50
0.60
0.70
0.80
0.90
1.00
1.10
1.20
1.30
-0.90
-0.80
-0.70
-0.60
-0.50
-0.40
-0.30
-0.10

Figure 7.

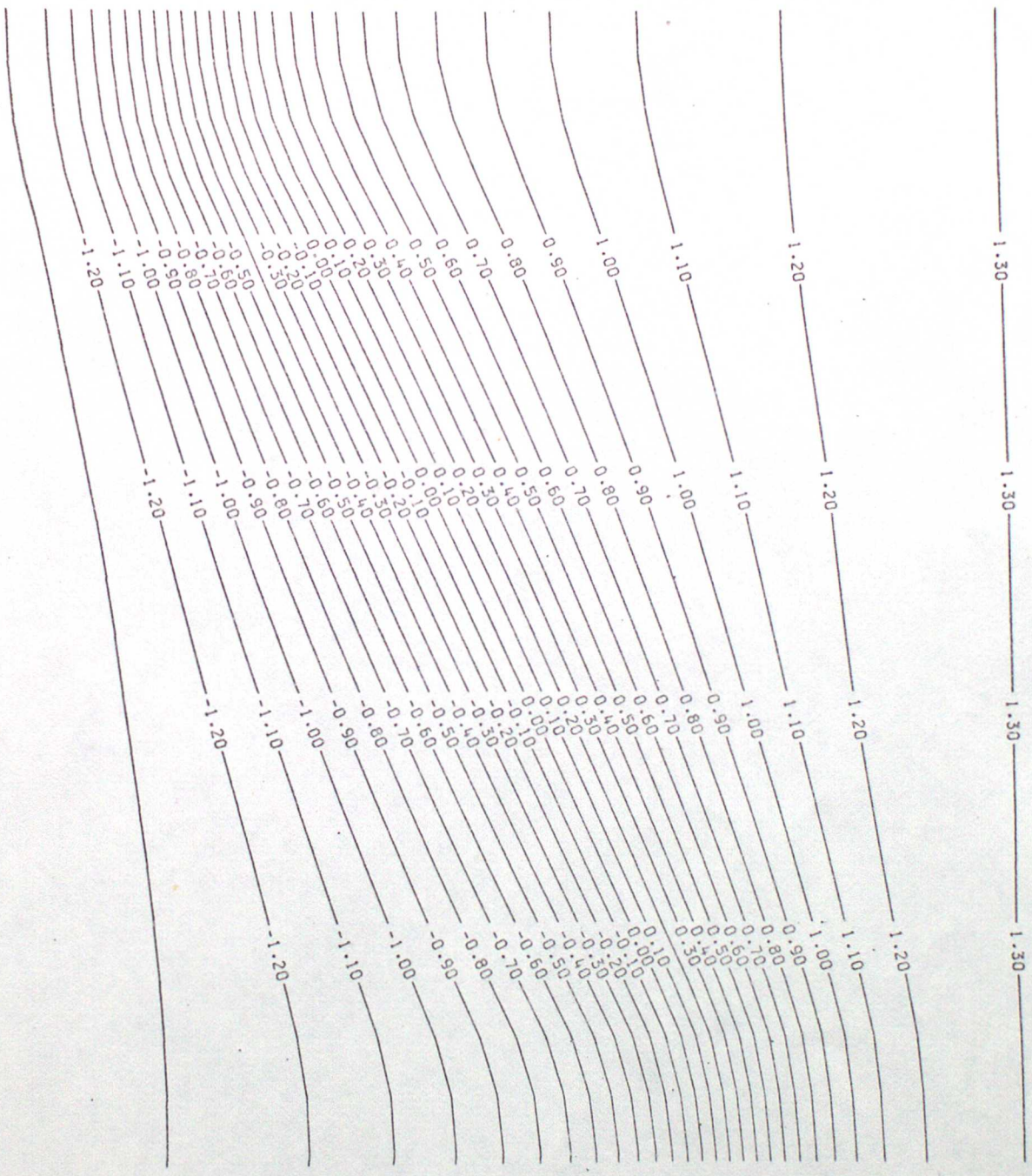
1.30
1.20
1.10
1.00
0.90
0.80
0.70
0.60
0.50
0.40
0.30
0.20
0.10
0.00
-0.10
-0.20
-0.30
-0.40
-0.50
-0.60
-0.70
-0.80
-0.90
-1.00
-1.10
-1.20

Figure 8.

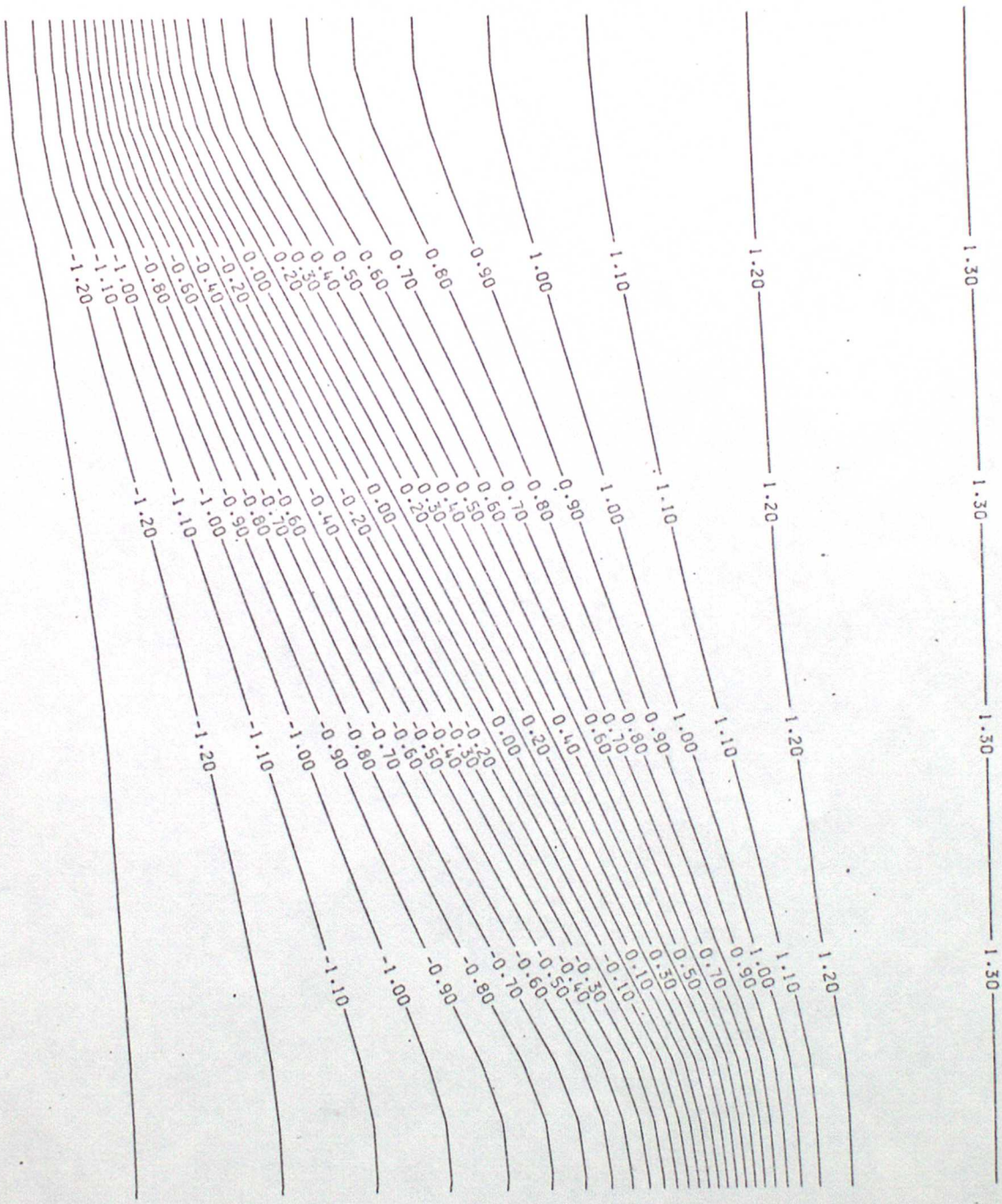
1.30
1.20
1.10
1.00
0.90
0.80
0.70
0.60
0.50
0.40
0.30
0.20
0.00
-0.20
-0.40
-0.60
-0.80
-1.00
-1.10
-1.20

Figure 9.

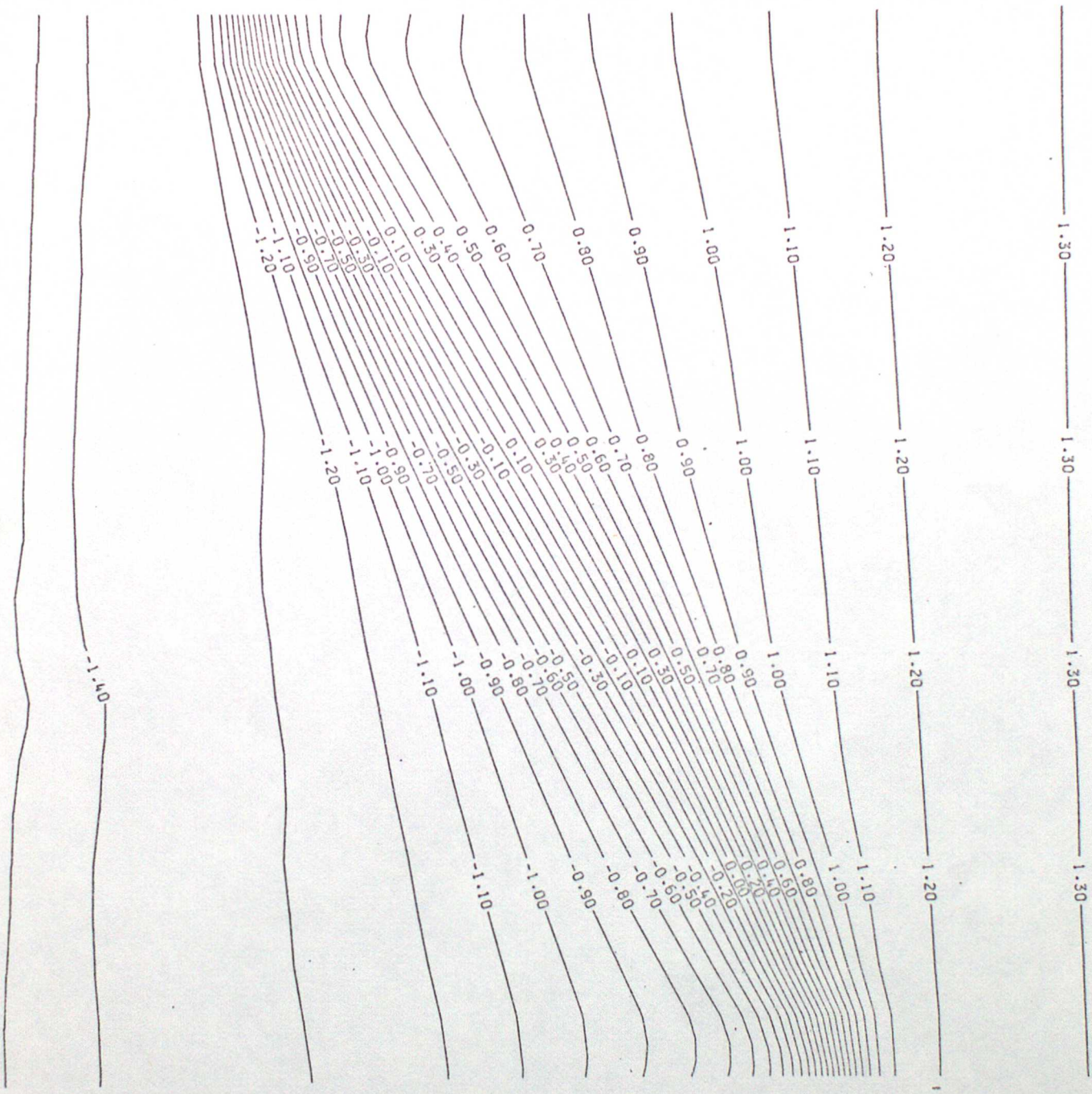
1.30
1.20
1.10
1.00
0.90
0.80
0.70
0.60
0.50
0.40
0.30
0.10
-0.10
-0.30
-0.50
-0.70
-0.90
-1.10
-1.20
-1.40

Figure 10.

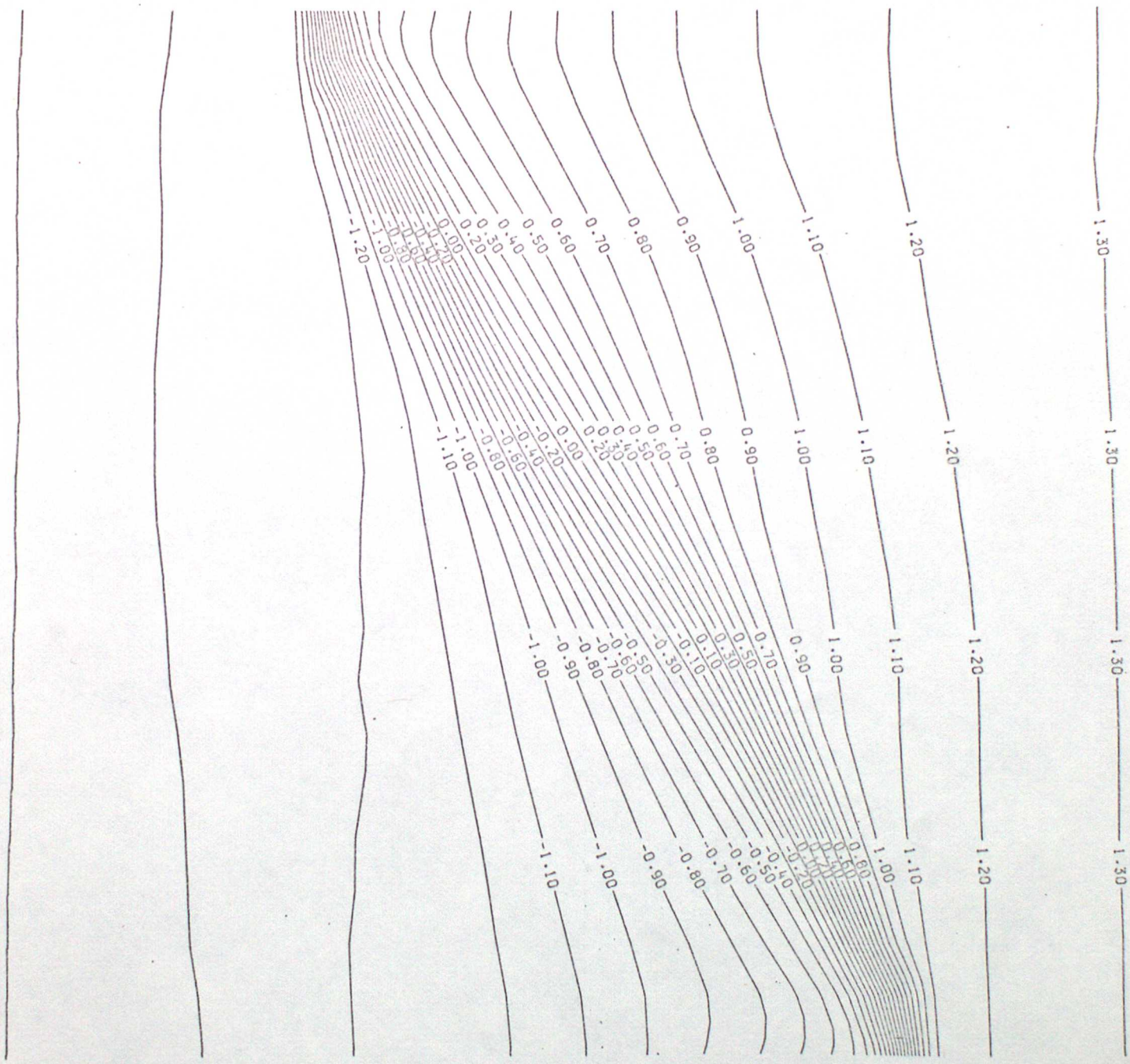
1.30
1.20
1.10
1.00
0.90
0.80
0.70
0.60
0.50
0.40
0.30
0.20
0.00
-0.20
-0.40
-0.60
-0.80
-1.00
-1.10
-1.20

Figure 11.

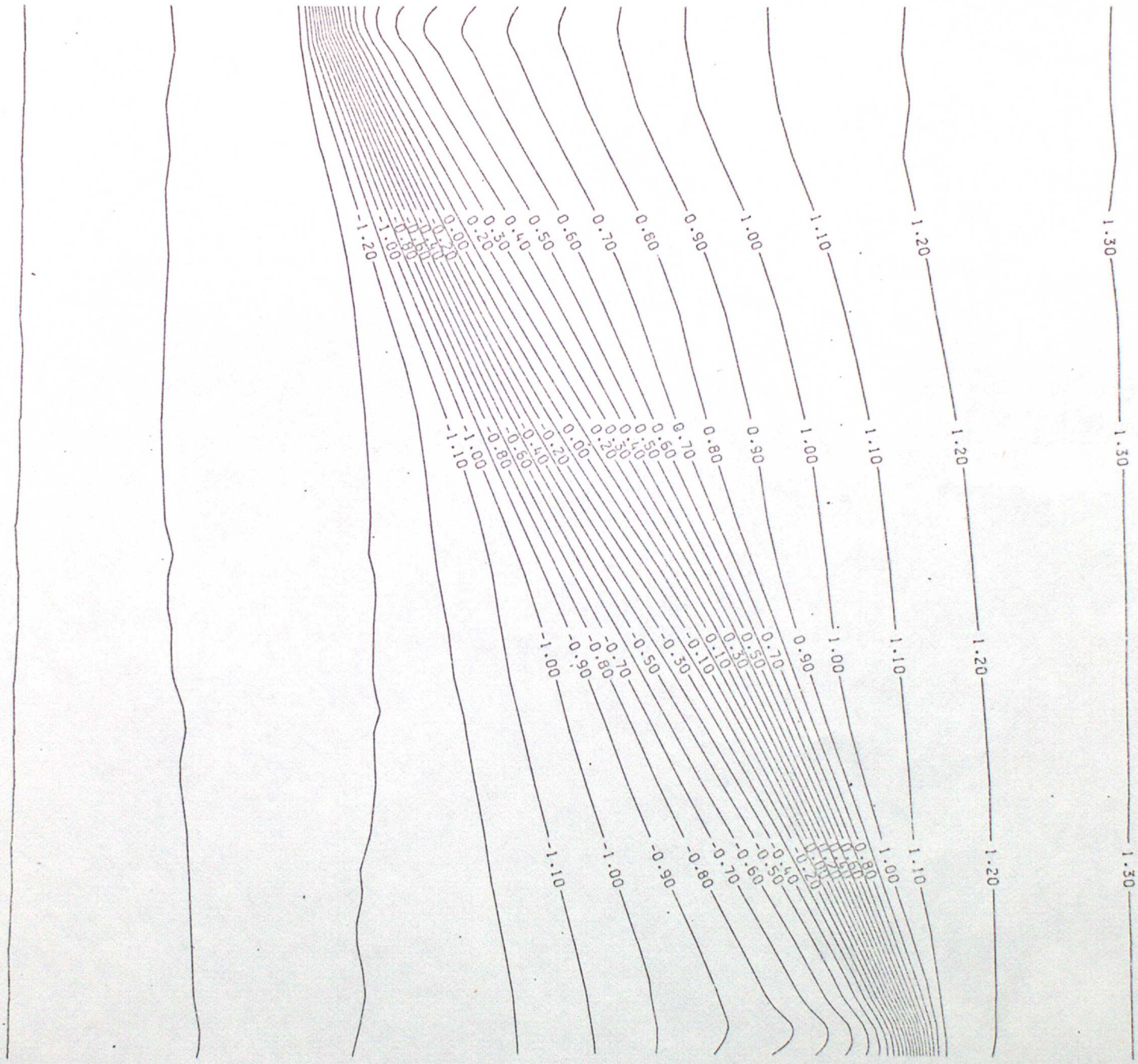
1.30
1.20
1.10
1.00
0.90
0.80
0.70
0.60
0.50
0.40
0.30
0.20
0.00
-1.00
-1.20
-0.10
-0.30
-0.50
-0.70
-0.90
-1.10
-0.80
-0.60
-0.40
-0.20

Figure 12.

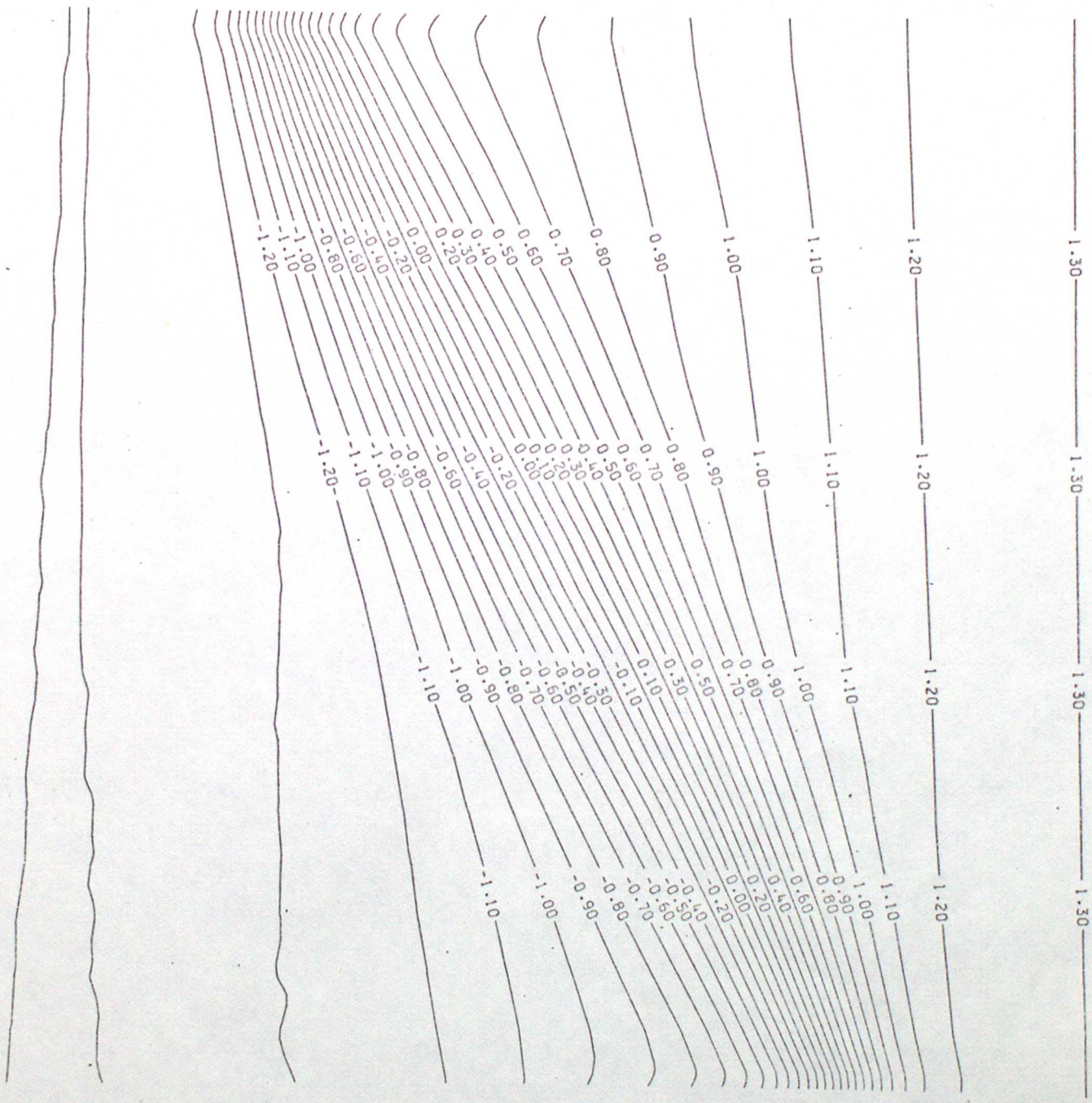
1.30
1.20
1.10
1.00
0.90
0.80
0.70
0.60
0.50
0.40
0.30
0.20
0.10
0.00
-0.10
-0.20
-0.30
-0.40
-0.50
-0.60
-0.70
-0.80
-0.90
-1.00
-1.10
-1.20

Figure 13.

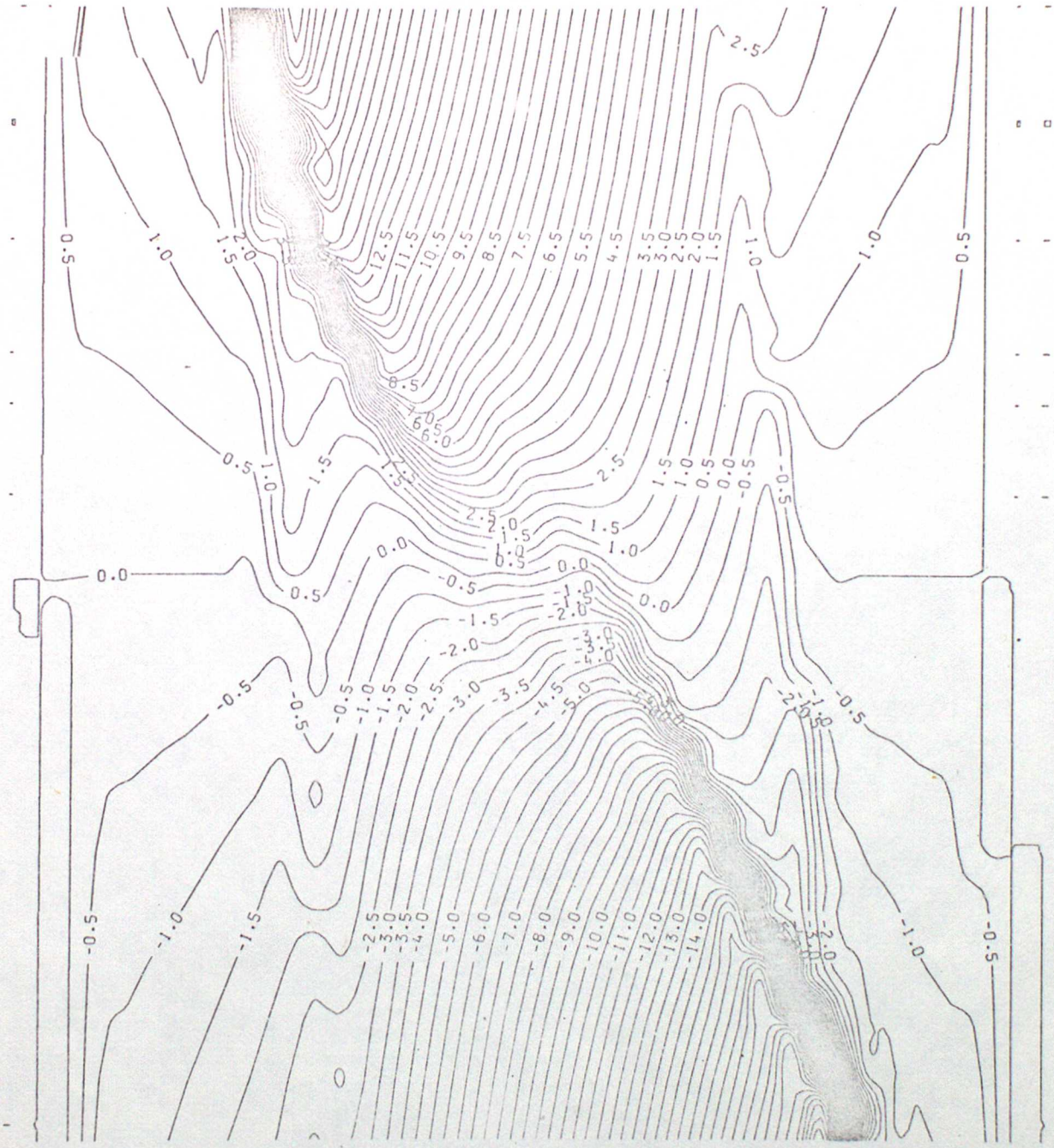
2.5
1.0
0.5
0.0
-0.5
-1.0
-1.5
-2.0
-2.5
-3.0
-3.5
-4.0
-4.5
-5.0
-5.5
-6.0
-7.0
-8.0
-9.0
-10.0
-11.0
-12.0
-13.0
-14.0
3.5
4.5
5.5
6.5
7.5
8.5
9.5
10.5
11.5
12.5
6.0

Figure 14.

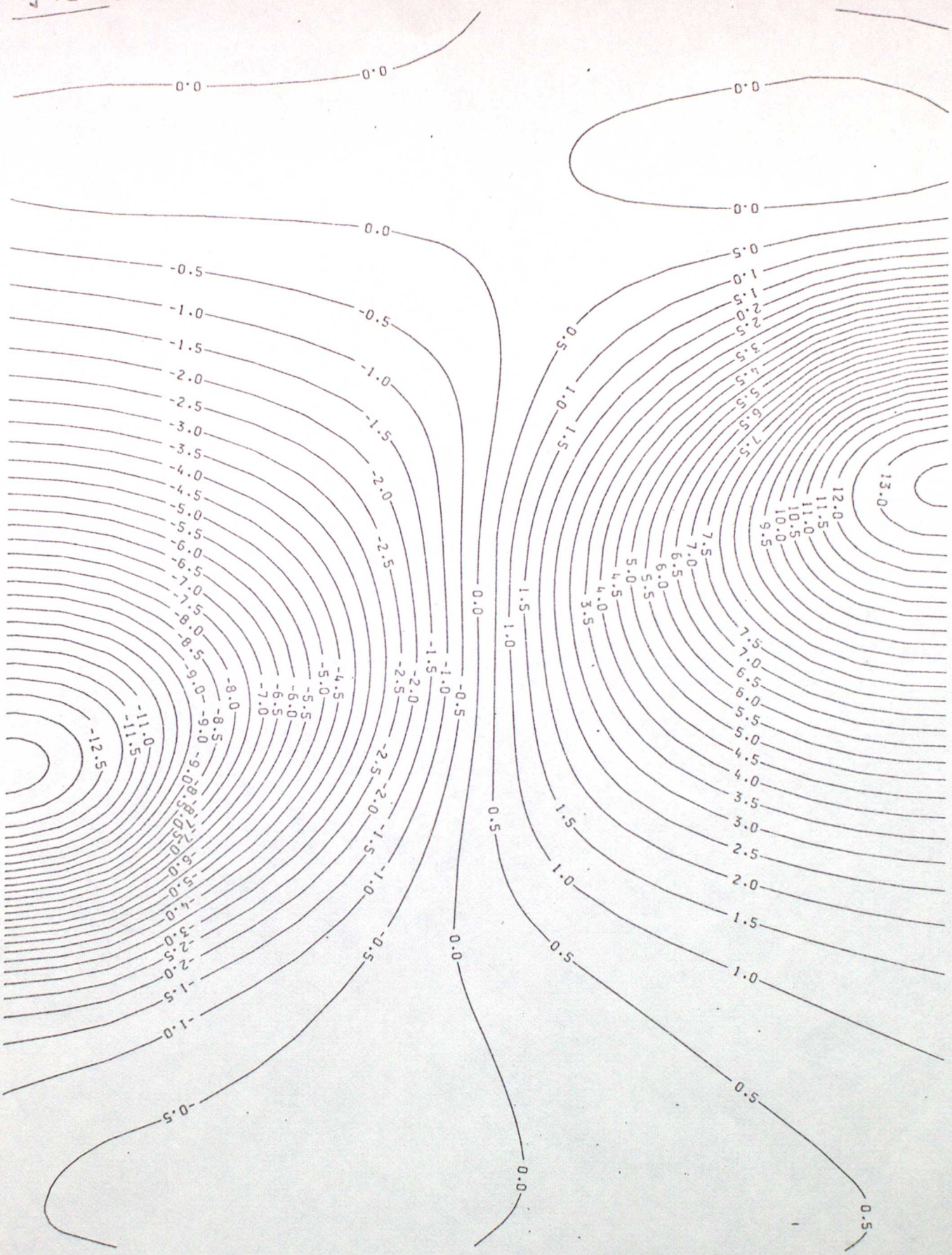
0.0
-0.5
-1.0
-1.5
-2.0
-2.5
-3.0
-3.5
-4.0
-4.5
-5.0
-5.5
-6.0
-6.5
-7.0
-7.5
-8.0
-8.5
-9.0
-9.5
-10.0
-10.5
-11.0
-11.5
-12.5
0.5
1.0
1.5
2.0
2.5
3.5
4.5
5.5
6.5
7.5
9.5
10.0
10.5
11.0
11.5
12.0
13.0

Figure 15.

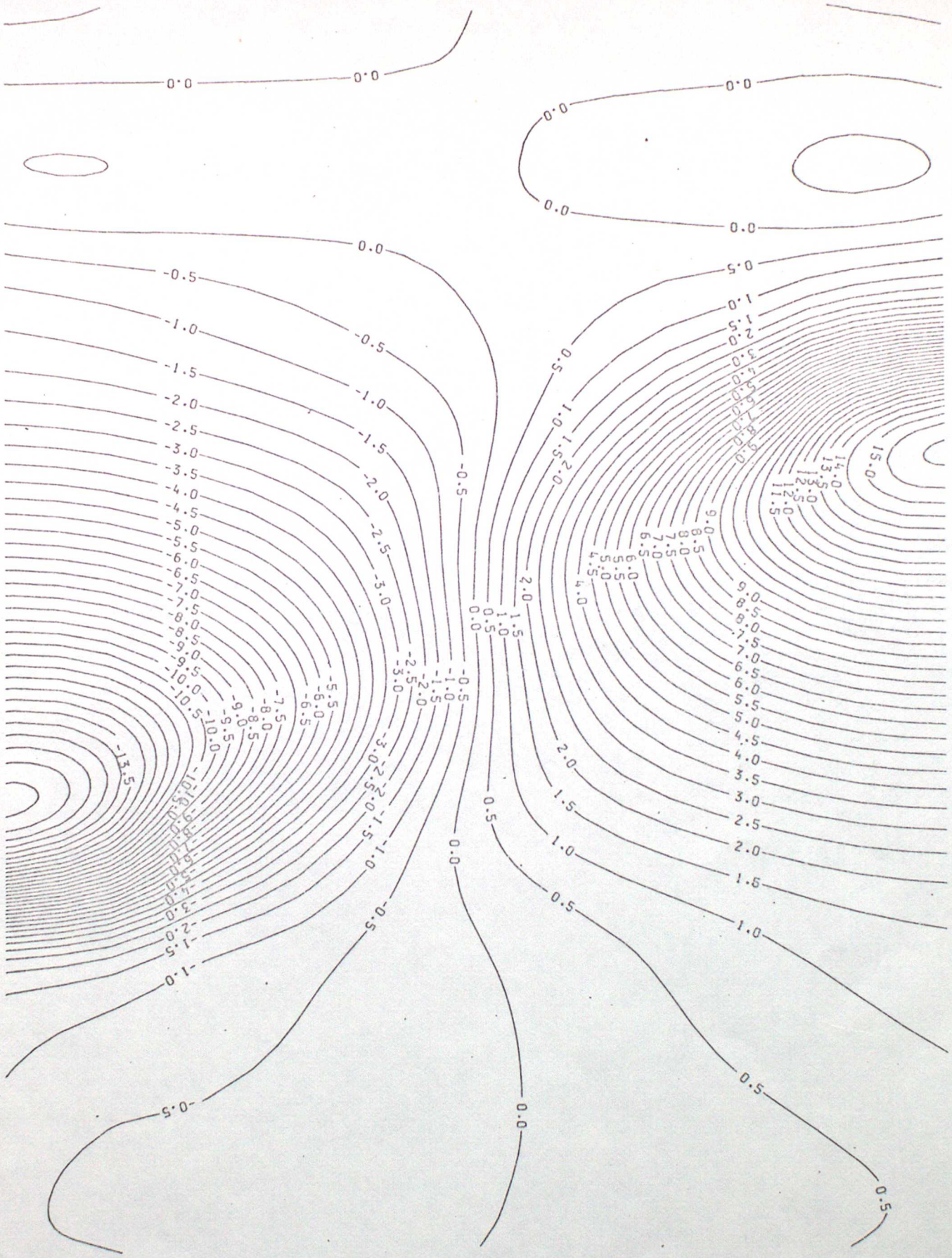
0.0
-0.5
-1.0
-1.5
-2.0
-2.5
-3.0
-3.5
-4.0
-4.5
-5.0
-5.5
-6.0
-6.5
-7.0
-7.5
-8.0
-8.5
-9.0
-9.5
-10.0
-10.5
-13.5
0.5
1.0
1.5
2.0
2.5
3.0
4.0
4.5
5.0
5.5
6.0
6.5
7.0
7.5
8.0
8.5
9.0
11.5
12.0
13.5
14.0
15.0

Figure 16.

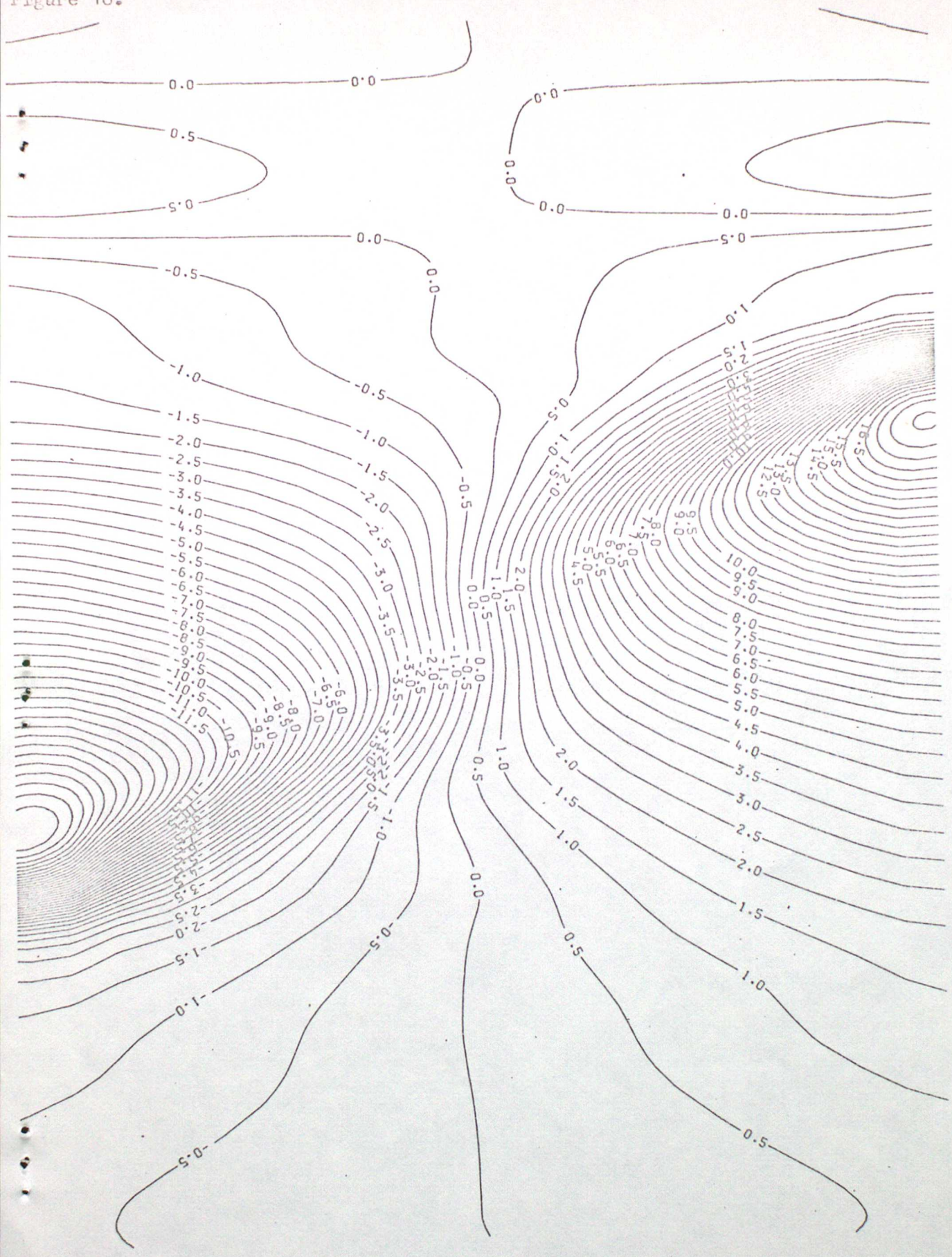

Figure 17.

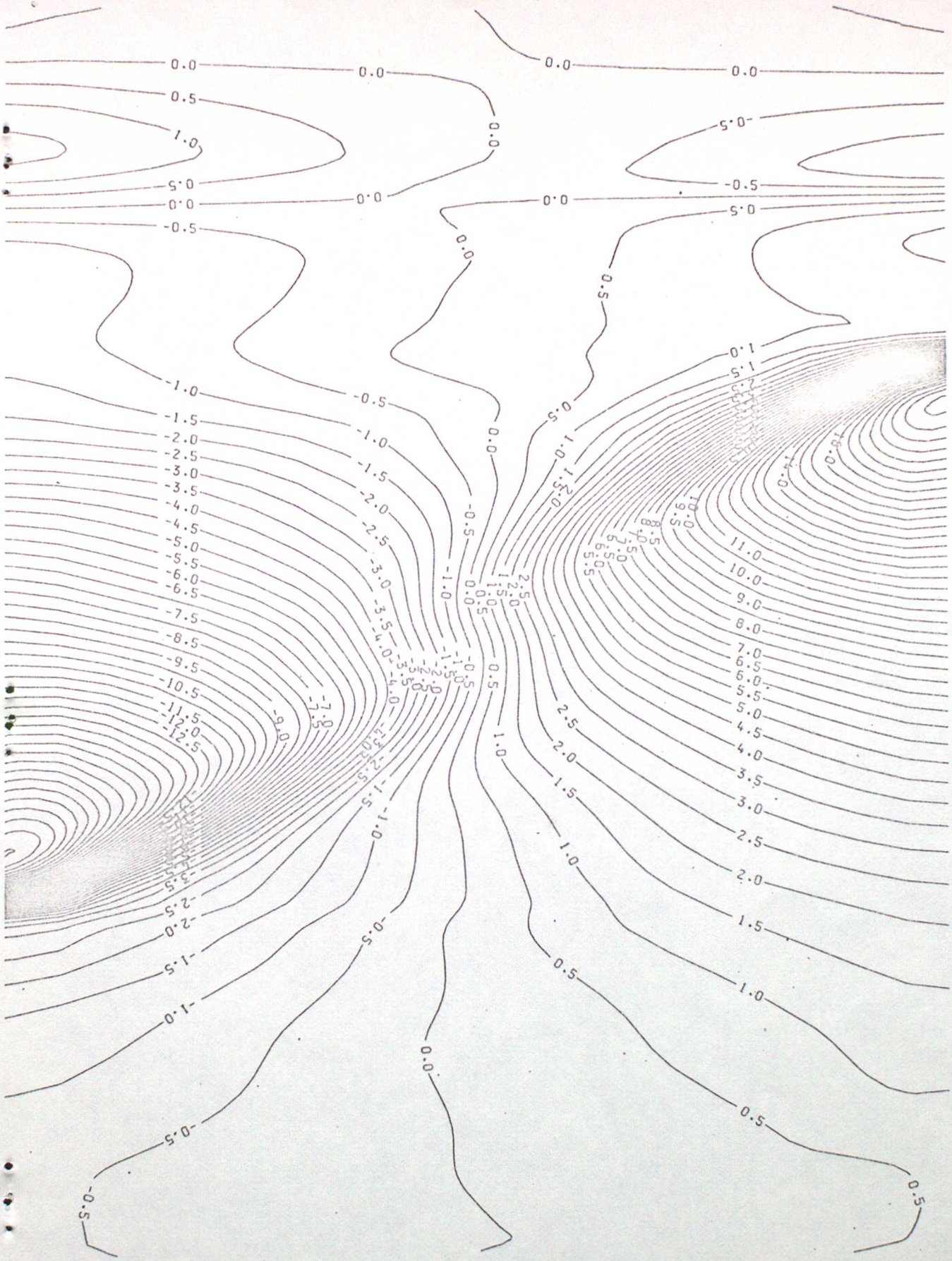
0.0
0.5
1.0
-0.5
-1.0
-1.5
-2.0
-2.5
-3.0
-3.5
-4.0
-4.5
-5.0
-5.5
-6.0
-6.5
-7.0
-7.5
-8.5
-9.0
-9.5
-10.5
-11.5
-12.0
-12.5
1.5
2.0
2.5
3.0
3.5
4.0
4.5
5.0
5.5
6.0
6.5
7.0
7.5
8.0
8.5
9.0
9.5
10.0
11.0
12.0

Figure 18.

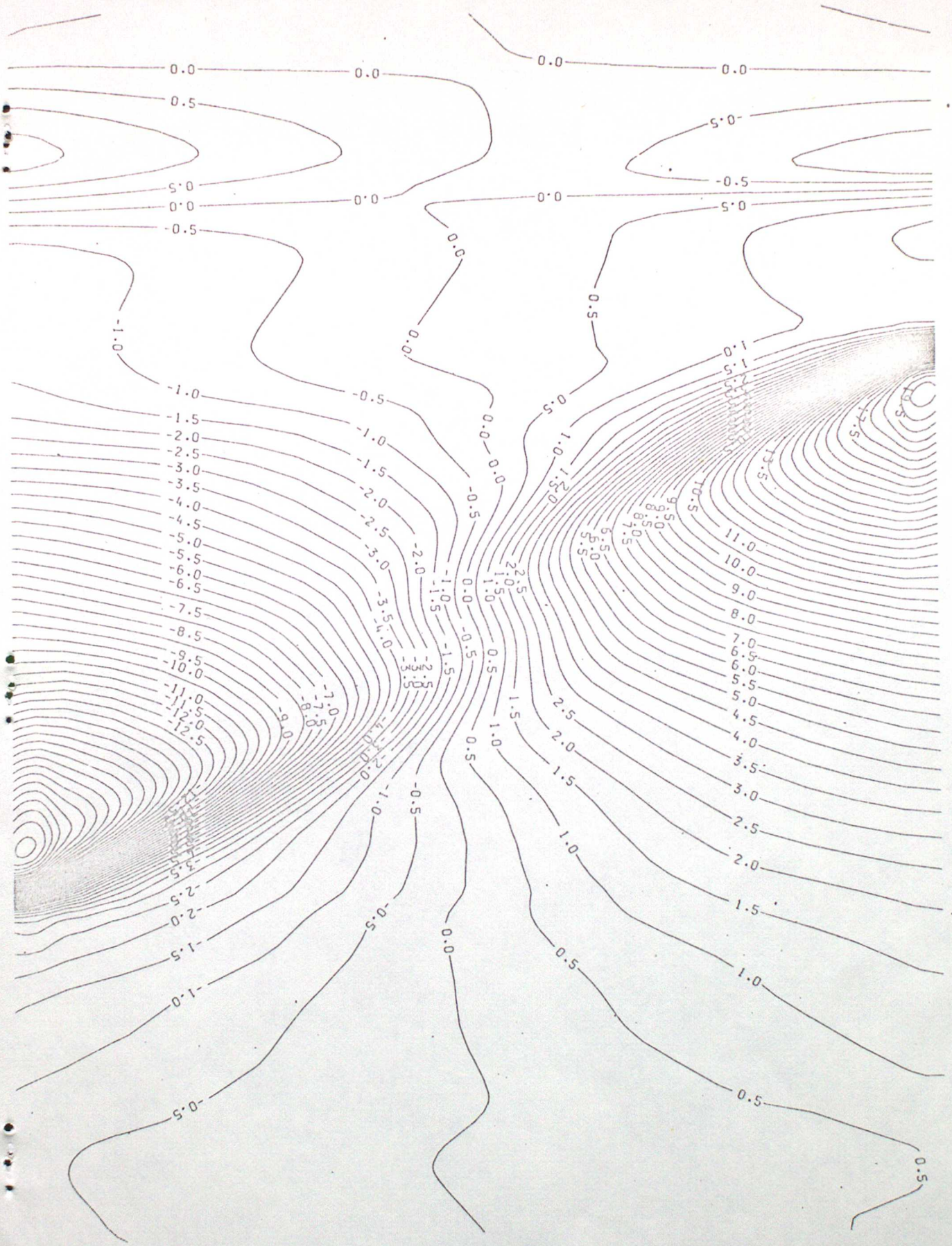
0.0
0.5
-0.5
-1.0
-1.5
-2.0
-2.5
-3.0
-3.5
-4.0
-4.5
-5.0
-5.5
-6.0
-6.5
-7.5
-8.5
-9.5
-10.0
-11.0
-11.5
-12.0
-12.5
1.0
1.5
2.0
2.5
3.0
3.5
4.0
4.5
5.0
5.5
6.0
6.5
7.0
8.0
9.0
10.0
11.0

Figure 19.

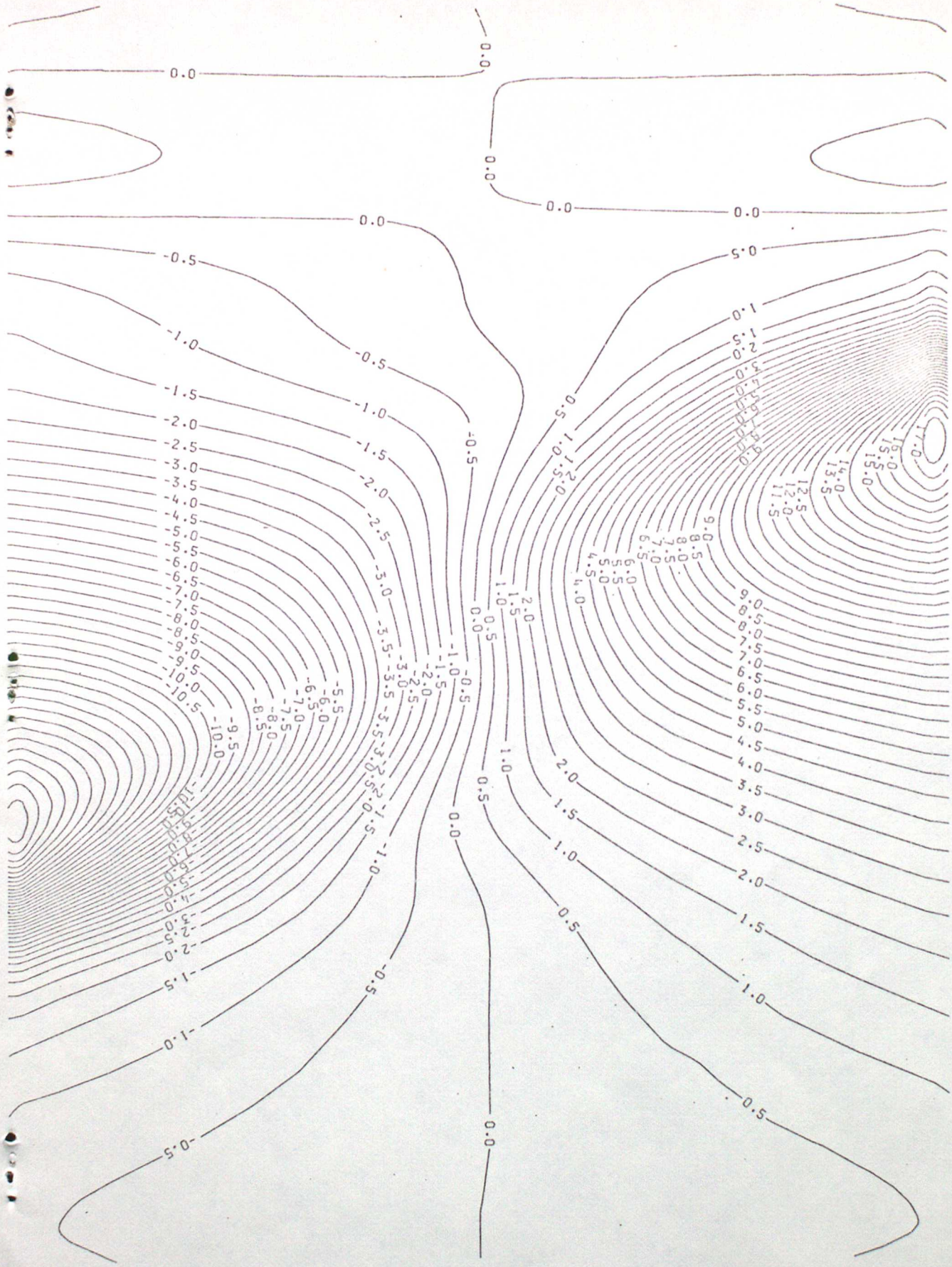
0.0
-0.5
-1.0
-1.5
-2.0
-2.5
-3.0
-3.5
-4.0
-4.5
-5.0
-5.5
-6.0
-6.5
-7.0
-7.5
-8.0
-8.5
-9.0
-9.5
-10.0
-10.5
0.5
1.0
1.5
2.0
2.5
3.0
3.5
4.0
4.5
5.0
5.5
6.0
6.5
7.0
7.5
8.0
8.5
9.0
9.5
10.0
10.5
11.0
11.5
12.0
12.5
13.0
13.5
14.0
14.5
15.0